Nanoscale

Accepted Manuscript

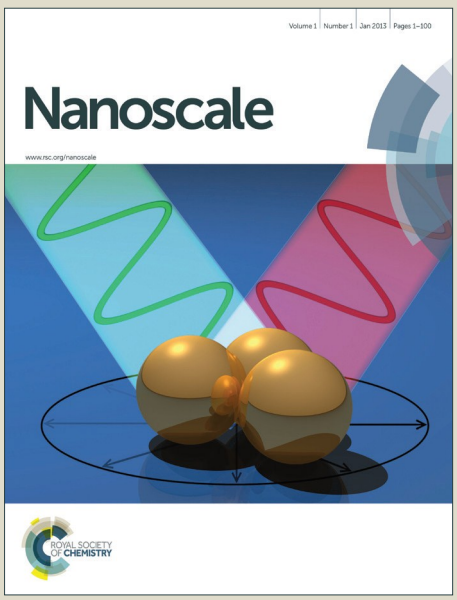

ROYAL SOCIETY OF CHEMISTRY

www.rsc.org/nanoscale

Cite this: DOI: 10.1039/xxxxxxxxxx

www.rsc.org/xxxxxx

Communication

Fabrication of Mesoporous Li_2S-C Nanofibers for High Performance Li/Li_2S Cells cathode†

Fangmin Ye[a], Yuan Hou[a], Meinan Liu[a], Wanfei Li[a], Xiaowei Yang[b], Yongcai Qiu[a], Lisha Zhou[a], Hongfei Li[a], Yijun Xu[a], and Yuegang Zhang*[a]

Received (in XXX, XXX) XthXXXXXXXXX 2015, Accepted Xth XXXXXXXXX 2015
DOI: 10.1039/xxxxxxxxxx

Li_2S electrode is a very promising cathode for Li-ion batteries. However, high voltage needed to activate Li/Li_2S cells represents a challenging problem. Here, we report for the first time a mesoporous Li_2S-C nanofiber composite with 72 wt. % Li_2S. The assembled Li/Li_2S cells showed a low and stable voltage plateau of 2.51V for the first charge and can deliver a high initial discharge capacity of ~ 800 mAh g^{-1}.

The current commercial Li-ion batteries (LIBs), such as $LiCoO_2$/graphite batteries, are widely used in portable electronics. However, the limited capacities for these electrodes cannot meet the increasing demand for many applications, such as electric vehicles and smart-grids. To develop high-energy storage devices, various anodes and cathodes have been investigated. Among them, low-cost, low-toxic element sulfur is believed to be one of the most promising candidates. As a cathode for lithium/sulfur (Li/S) battery, its conversion reaction can reversibly incorporate two electrons per sulfur atom, thus showing high theoretical specific capacity of 1675mAh g^{-1} and high specific energy of 2600wh kg^{-1}.[1,2] Nonetheless, the lithium metal anode imposes several serious safety issues,[1,3,4] due to its high reactivity and the possible growth of lithium dendrites upon cycling[5,6]. To avoid using lithium metal anode, lithium-containing cathode need to be used.

Lithium sulfide (Li_2S), a fully lithiated sulfur compound as an alternative cathode material, not only shows a high theoretical specific capacity of 1166mAh g^{-1}, but also can be paired with some promising lithium metal-free anodes, such as graphite[7,8], tin[9,10] and silicon[11-13]. Motivated by its potential, various methods, including high-energy ball-milling,[13-18] solution-based chemistry,[19-23] decomposition of polymer-Li_2S/Li_2S_x,[24-26] in-situ synthesis, [9,12,27] were developed to fabricate Li_2S and Li_2S-C composites. A Li_2S-carbon sandwiched electrode has also been studied.[28] However, one-dimensional (1D) Li_2S-C composite has not been reported before.

Due to its high electronic and lithium ion insulating nature, Li_2S is usually considered to be electrochemically inactive. Previous reports indicate that Li_2S-C composite cathodes need to be activated before normal cycling. Cui et al[16] have showed that there is a potential barrier during the initial charge to fully convert Li_2S into sulfur, which can be overcome by applying a high cutoff voltage or a low charge current density. To decrease the potential barrier of a Li_2S cathode and improve lithium storage capability, our group[17] reported a high-energy ball-milled Li_2S-C composite with a low potential barrier and a high initial discharge capacity, which was attributed to the small Li_2S grain size encapsulated by carbon matrix. Archer et al[24] reported that a low potential barrier of a Li_2S cathode could be achieved by Li-N interaction. More recently, Chen et al[29] reported the N-doped carbon encapsulated Li_2S composite showed a low potential barrier and charge voltage plateau. It is also found that the charge voltage plateau and/or the activation voltage in most reports were unstable, probably due to the uneven Li_2S grains and unstable conductivity network. Generally, a high activation voltage of 4.0V is normally used thus far. Under such a high voltage, ether-based electrolyte solution (e.g., LiTFSI in DOL/DME and $LiNO_3$ additives) are thought to be unstable.[30] Therefore, it is urgently needed to design a Li_2S composite structure with a low activation voltage and excellent electrochemical performance including high specific capacity and high Coulombic efficiency.

Herein, for the first time to the best of our knowledge, a novel 1D lithium sulfide-carbon (Li_2S-C) nanofiber (NF) composite was prepared by combining electrospinning and subsequent pyrolysis technology. The Li_2S-C NFs, with a characteristic structure of tens of nanometer-sized Li_2S nanoparticles uniformly embedded in porous carbon layers, can greatly improve the lithium transport kinetics in the Li_2S cathode because of the nanoscaled Li_2S particles and their good electrical contact with the mesoporous carbon matrix. As a result, the Li/Li_2S cells assembled with the Li_2S-C NFs as a cathode display two striking features for initial charge process, i.e., a low initial activation potential of 2.57V, a low and stable charge voltage plateau (~2.51V). The cells can also deliver a high initial specific capacity of ~800 mAh g^{-1} (based on the mass of Li_2S) and a reversible capacity of ~510 mAh g^{-1} after 100 cycles at a rate of 0.5C.

[a]*i-LAB, Suzhou Institute of Nano-Tech and Nano-Bionics, Chinese Academy of Sciences, Suzhou, 215123, P. R. China. E-mail : ygzhang2012@sinano.ac.cn Tel.: +86 - 512 - 62872772*
[b]*School of Materials Science and Engingeering, Tongji University, Shanghai 200092, P. R. China.*

†Electronic supplementary information (ESI) available: Synthesis, characterization, calculation of Li_2S content and electrochemical measurements of Li_2S-C nanofibers. See DOI: 10.1039/xxxxxxxxxx.

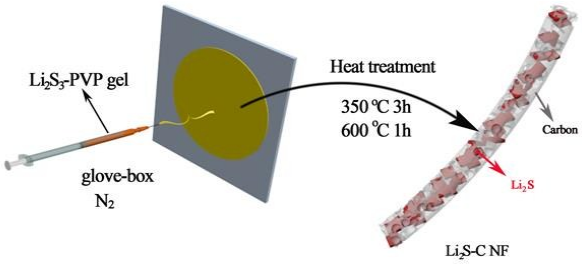

Figure 1 Schematic representation of the fabrication process of the Li_2S-C NFs by electrospinning and subsequent heat treatment.

The Li_2S-C NFs were fabricated according to the experimental procedure shown in Figure 1 (see Electronic Supplemetary Information for the detailed experimental steps). The commercial Li_2S, sulfur and polyvinyl pyrrolidone (PVP) were dissolved into ethanol to form a transparent brown-yellow Li_2S_3-PVP precursor gel. The Li_2S_3-PVP NFs were prepared from the precursor gel by electrospinning. It should be noted that ethanol was used here as the solvent instead of DMF reported previously[24] to form a uniform Li_2S_3 because of its low boiling point and low toxicity, which could be beneficial to the electrospinning process. The as-spun NFs were annealed at 350°C for 3h and subsequently 600°C for 1h to obtain final Li_2S-C NFs.

The structure and composition of the as-spun composite were investigated by XRD, SEM and XPS, and the results are shown in Figure S1b and Figure S2-S3. Figure S1b shows no obvious diffraction peak in XRD pattern, suggesting that the as-spun composites are amorphous. A broad peak corresponding to Li_2S_3 can be observed in XPS pattern shown in Figure S2. Based on above results and the mole ratio of Li_2S and sulfur for gel of electrospinning, the as-spun samples are determined to be Li_2S_3-PVP. Figure S3 shows that the as-spun composite consists of numerous NFs. After annealed at 350°C for 3h, the Li_2S_3 can be transformed into Li_2S, as evidenced by XRD pattern in Figure S1c. All the diffraction peaks marked with asterisk shown in the pattern can be indexed to a cubic Li_2S (Cassiterite, Joint Committee on Powder Diffraction Standards (JCPDS) card No.26-1188), suggesting that Li_2S_3 can be decomposed into Li_2S at 350°C. A similar experimental result was also reported previously[24]. To produce the final Li_2S-C composites, the composite was subsequently carbonized at 600 ℃ for 1h under Ar. As shown in Figure S1d, all diffraction peaks marked with asterisk belong to cubic Li_2S, and the intensity of these peaks is much stronger than those in Figure S1c, indicative of the higher crystallinity of Li_2S after annealing at a higher temperature.

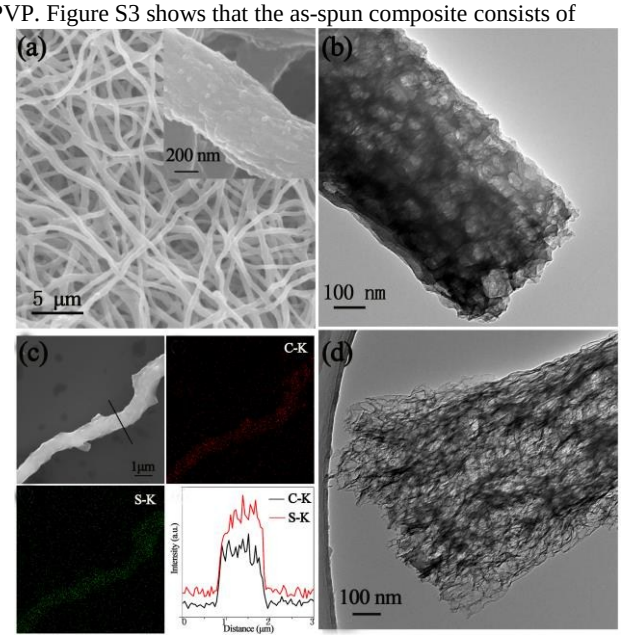

Figure 2 (a) SEM image of Li_2S-C NFs and a Li_2S-C NF (inset), (b) TEM image of a Li_2S-C NF, (c), Top-left: SEM image of a Li_2S-C NF; Top-right and bottom-left: the corresponding EDX elemental maps for carbon and sulfur; Bottom-right: normalized line-scanned EDX intensity for Carbon (red) and Sulfur (black) along the black line show in the top-left,(d) TEM image of a carbon NF matrix after Li_2S removed.

Figure 2a displays a typical low magnification SEM image of the Li_2S-C NFs. The 1D fiber-like structure can be well maintained after heat treatment at 600°C. In addition, some exposed Li_2S particles were clearly observed on the surface of NFs from the high magnified SEM image (in the inset of Figure 2a). These exposed grains size of Li_2S is about 60-80nm and the diameter of NFs is around 0.5~1μm. TEM technique was also used to characterize the inner structure of the Li_2S-C NFs. As shown in Figure 2b, a porous structure of Li_2S-C NFs can be clearly observed. The formation of pores is probably due to the evaporation of sulfur and the volumetric shrinkage from Li_2S_3 to Li_2S. To further determine the distribution of Li_2S in the Li_2S-C NFs, the energy dispersive X-ray (EDX) elemental maps and a line scan across a single NF are shown in Figure 2c for carbon and sulfur. The results indicate that carbon and sulfur are homogeneously distributed throughout the NFs. The Li_2S content in the Li_2S-C NFs was determined to be about 72.2 wt. % (see Electronic Supplementary Information for detailed calculation).

To further identify the inner structure of the conductive carbon matrix, Li_2S nanoparticles were removed by immerging the Li_2S-C composite NFs in a mixture of ethanol and deionized water. As shown in Figure 2d and Figure S4, the carbon matrix exhibits a unique intertwined network structure, which provides excellent electron conduction paths for the nanometer-sized Li_2S particles homogeneously embedded in the conductive carbon network. The Brunauer-Emmett-Teller (BET) surface area and pore size distribution of the carbon NFs were characterized by adsorption/desorption isotherms. Figure 3a exhibits a typical feature of type IV physisorption isotherms with a BET surface area of 272m^2 g^{-1}. Also, the H4 type loop suggests narrow slit-like pores formed by sheet-like carbon layers, which is consistent with the results shown in Figure 2d. Figure 3b shows that the pores in the carbon fibers with the absence of Li_2S are in the range of 5~70nm, suggesting that the size of Li_2S particles in the

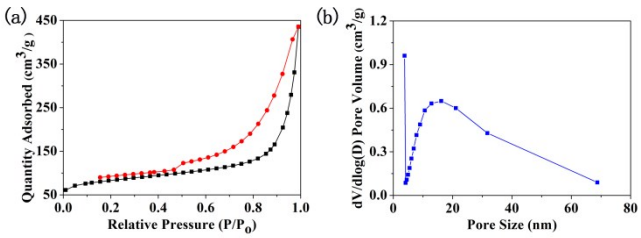

Figure 3 (a) N_2 adsorption-desorption isotherms and (b) pore size distribution of the carbon NFs after Li_2S removed

NFs is below 70nm. The mesopores in the NFs probably arises from the evaporation of sulfur through the conversion Li_2S_3 to Li_2S in the as-spun NFs upon heat treatment, leading to the formation of mesoporous structures of the carbon matrix.

To examine the effect of the unique Li_2S-C NF mesostructure on Li/S batteries, we investigated the electrochemical properties of the material assembled in coin cells (see Electronic Supplementary Information for Electrochemical Measurements). The electrochemical reaction of the Li_2S-C NFs was first investigated by the cyclic voltammetry (CV). Figure 4a shows an initial CV curves scanned from open circuit voltage to 3.8V at a scan rate of 0.025mV s^{-1}. It is found that the initial cathodic peak centers at 2.77V, is distinctly lower than that of some reported Li_2S-C cathode which is generally higher than 3V[25, 28], indicating a delithiation reaction with lower energy barrier in our Li_2S-C cathode. Thus, a cutoff voltage of 3.2V is enough to complete the initial delithiation reaction. Figure 4b shows initial oxidation process scanned to 3.2V at various scan rates of 0.001, 0.005, 0.025 and 0.1mV/s, respectively. Despite of a shift of the cathodic peaks to higher voltage with increasing scan rates, all the cathodic peaks still appear below 3V, meaning a low activation voltage for Li_2S-C NFs cathode. In the subsequent CV scanning, the cells were cycled at a voltage range of 1.7~2.8V. Figure 4c shows the CV results for 5 cycles at a scan rate of 0.025mV s^{-1}. The initial oxidation process was in agreement with the result in Figure 4b. In the first anodic reaction process, two strong reduction peaks were observed. A peak at 2.33V can be ascribed to the formation of Li_2S_8 from the reaction of S_8 and lithium ions, while the relatively stronger peak centred at 2.08V, is assigned to the formation of Li_2S_2 and/or Li_2S. In the second oxidation sweep, two oxidation peaks indicate the reversible conversion of Li_2S to polysulfides (e.g. Li_2S_4, Li_2S_6 and Li_2S_8) and polysulfide to sulfur, respectively. The subsequent redox processes show a very stable cycling profile, meaning that the cells with the Li_2S-C NFs cathode exhibit high reversibility of redox reactions and a stable structure upon cycling(Figure S5). Furthermore, it can be seen that the locations of the first anodic peak and the first cathodic peak almost coincide at about 2.32V. The small voltage difference between the anodic and cathodic peaks further indicates that the structure of our Li_2S-C NFs is electrochemically stable, and they could provide excellent electric quality and high round-trip efficiency.

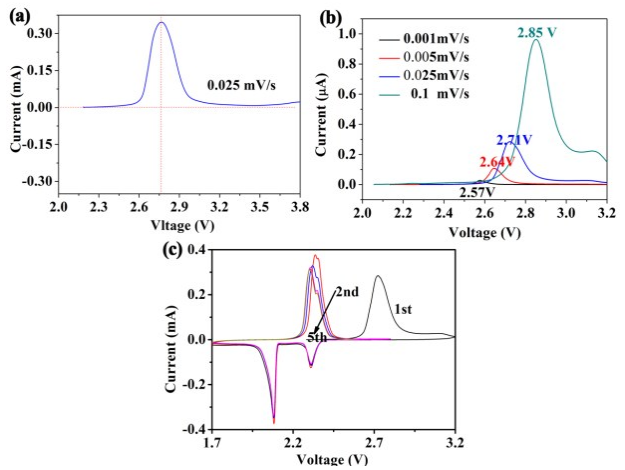

Figure 4 Cyclic voltammograms (CV) of the Li_2S-C NF cathode. (a) Initial oxidation to 3.8V at a scan rate of 0.025mV s^{-1}, (b) initial oxidation to 3.2V at various scan rates, (c) CV for 5 cycles at a scan rate of 0.025 mV s^{-1}.

The charge/discharge cycling performance of the Li_2S-C NF cathode was studied at a constant current. The initial charge and discharge current rate was 0.025C (1C = 1166mA g^{-1} by Li_2S weight) with a cutoff voltage to 3.2V, then the cell was cycled at a current rate of 0.5C in a cutoff voltage window between 1.7 and 2.8V. Figure 5a shows the capacity vs voltage profiles of the 1st, 2nd and 3rd cycle. In the beginning of first charge process, it can be found that the voltage increases quickly to 2.57V and then decreases, indicating a low activation voltage of only 2.57V for the Li_2S-C NF cathode. Also, a stable voltage plateau of 2.51V lasts a long charge process, suggesting a stable structure and uniform Li_2S grains size in the Li_2S-C NFs. The subsequent charge/discharge curves of the 2nd and 3rd cycles are in agreement with the CV results. It should be noted that the Li/Li_2S-C NF cells also show low activation voltages of 2.54 and 2.67V at a lower or a higher charge rate of 0.01C and 0.1C, respectively (Figure S6). These results can be ascribed to the improvement of charge transport kinetic of Li_2S NF cathode due to the following two effects. One is the synchronous formation of Li_2S and carbon phases during the pyrolysis of Li_2S_3-PVP NFs, which leads to highly conductive carbon networks and ultrafine Li_2S grains. Another is the generation of mesopores during the decomposition of Li_2S_3, which facilities the electrolyte penetrating into the NFs. These effects are beneficial for the transport of ions and electrons, as well as the formation of polysulfides, thus leading to a low activation voltage.

To further understand the unique low-voltage activation process of the Li_2S-C NF cathode, electrochemical impedance spectra (EIS) at different stages of the initial charge process were collected. Figure 5b shows a curve of voltage versus capacity for the initial charge process at a rate of 0.025C, where the labels (A ~ M) indicates different EIS test points. As shown in Figure 5c and 5d, all the EIS curves consist of one depressed semicircle at a

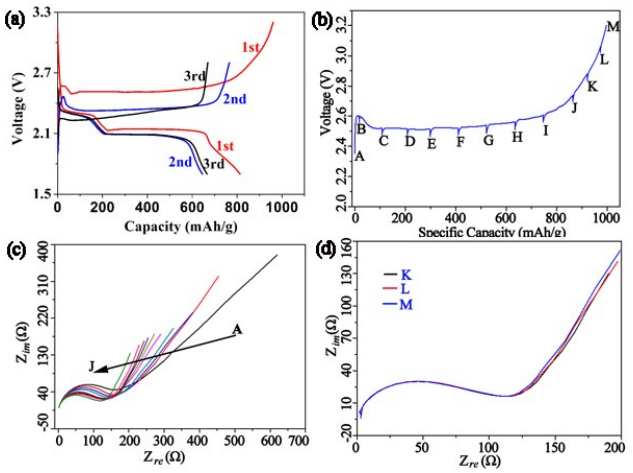

Figure 5 (a) Galvanostatic charge-discharge curves of Li_2S-C NF cathode at a rate of 0.025C (initial charge/discharge) and 0.5C (subsequent cycles), respectively. (c) Initial charge curves for voltage vs capacity at a rate of 0.025C. (A~M marked means a test point). (c) and (d) show the EIS collected at different test point .

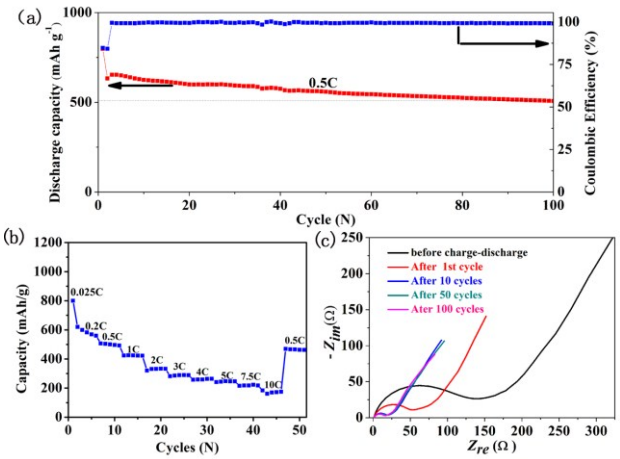

Figure 6 (a) Cycling performance and the Coulombic efficiencies of the Li_2S-C NFs cathode at a current rate of 0.025C (initial charge/discharge) and 0.5C (subsequent cycles), respectively. (b) Rate performance of Li_2S-C NF cathode. (c) EIS of the as-assembled half-cell and after 1st,10th,50th and 100th cycles, obtained in the frequency range from 0.01Hz to 100 kHz.

high/medium frequency and an inclined line at low frequency. The semicircle in the EIS reduces from A to C (Figure 5c), suggesting that the charge transfer resistance at the surface gradually decreases due to the formation of polysulfides. The slope of line in the low frequency region increases gradually, meaning that the lithium-ion diffusion process within the electrodes is also improved. These behaviors are consistent with that the voltage rises to the peak of the low activation voltage 2.57V at B point and then decrease to 2.51V at C. However, from C to J, the voltage increases very slowly, and the corresponding EIS curves from C to J (Figure5c) shows a slowly decreasing semicircle diameter and a relatively constant slope of the inclined lines, suggesting a stable electrochemical reaction occurs. The EIS from K to M coincides (Figure 5d), indicating that the delithiation for Li_2S-C cathode is almost completed. As previously discussed, the homogeneous distribution of the nanometer-sized Li_2S particles in carbon matrix and the existence of mesopores in the Li_2S-C NFs greatly improved the contacts of Li_2S particles, electrolyte, and carbon network, which led to a good electrical conductivity and high utilization of active materials, and realized the low activation voltage.

Figure 6a shows the discharge capacities vs. cycle numbers for a Li/Li_2S-C NF cell. The initial discharge capacity is ~800mAh g^{-1} at a rate of 0.025C and the initial Coulombic efficiency (CE) is ~ 84%. From the 2nd to the 100th cycle under 0.5C, the discharge capacity decreases slowly, but can still remain 510mAh g^{-1} after 100 cycles. Besides, the cell shows a high and stable CE, which is close to ~100% after the 2nd cycle. The good cycling performance can be ascribed to the excellent reversibility and the effective use of active materials due to the mesoporous structure and the excellent conductive network of Li_2S-C NFs.

The advantages of this material were further demonstrated by its rate performance. As shown in Figure 6b, the reversible capacity of a Li/Li_2S-C NF cell only gradually decreases with increasing current density. At a rate of 0.5C, the cell delivers a specific capacity of 500mAh g^{-1}. Even at high rates of 5C and 10C, the specific capacities can still remain 250 and 170mAh g^{-1}, respectively. When the current rate is switched back to 0.5C, the capacity can be restored to ~500 mAh g^{-1}, indicating an extraordinary stability of the electrode structure upon cycling. Moreover, the stable structure is also supported by the EIS data after charge/discharge cycles. Figure 6c shows the Nyquist plots measured after various charge/discharge cycles. The semicircle diameter decreases during the initial several cycles and then keeps a stable value roughly after the 10th cycle, indicating the solid-electrolyte interface resistance and the charge-transfer resistance stablize after 10 cycles. On the other hand, the slope of inclined line at low frequency region barely changes from its initial value, which indicates a stable lithium-diffusion process within the electrode. These results provide clear evidences that the Li_2S-C NFs enables very stable charge-transfer processes, which leads to their good cycling performance after a low voltage activation.

Conclusions

In conclusion, we synthesized a mesoporous Li_2S-C NF structure by combining electrospinning and subsequent pyrolysis processes. The synchronous formation of Li_2S and carbon due to the decomposition of Li_2S_3-PVP NFs leads to the uniformly distributed ultrafine Li_2S grains in highly conductive carbon NF matrix. Moreover, the mesopores in the Li_2S-C NFs resulting from the evaporation of sulfur during pyrolysis facilitate lithium ion transport in the active materials, thus favouring the formation of polysulfides and utilization of the active materials. The unique structure enabled a low activation potential of ~ 2.57V for a Li/Li_2S cell and an extraordinarily stable initial charge plateau of ~2.51V. The results demonstrated here could lead to a better electrode material design for more practical lithium metal-free Li_2S batteries.

Acknowledgement

Financial support from China postdoctoral science foundation (No. 2014M551677), National Natural Science Foundation of China (No.21433013, No.51402345, No. 21403287), Suzhou science and technology development program (ZXG2013002) and Natural Science Foundation of Jiangsu Province, China (No. BK20140383).

References

1. L. Ji, M. Rao, H. Zheng, L. Zhang, Y. Li, W. Duan, J. Guo, E. J. Cairns, Y. Zhang, J. Am. Chem. Soc., 2011, **133**, 18522.
2. M. Song, E. J. Cairns, Y. Zhang, Nanoscale, 2013, **5**, 2186.
3. Xu, K., Chem. Rev., 2004, **104**, 4303.
4. R. Chen, T. Zhao, F. Wu, Chem. Comm., 2015, **51**, 18.
5. D. Aurbach , Y. Cohen, J. Electrochem. Soc., 1996, **143**, 3525.
6. D. Aurbach, E. Zinigrad, Y. Cohen, H. Teller, Solid State Ionics, 2002, **148**, 405.
7. G. Ma, Z. Wen, M. Wu, C. Shen, Q. Wang, J. Jin, X. Wu, *Chem. Commun.*, 2014, **50**, 14209.
8. J. Brückner, S. Thieme, F. Böttger-Hiller, I. Bauer, H. T. Grossmann, P. Strubel, H. Althues, S. Spange, S. Kaskel, *Adv. Funct. Mater.*, 2014, **24**, 1284.
9. S. Zheng, Y. Chen, Y. Xu, F. Yi, Y. Zhu, Y. Liu, J. Yang, C. Wan, *Acs nano*, 2013, **7**, 10995.
10. J. Hassoun, B. Scrosati, *Angew. Chem. Int. Ed.*, 2010, **49**, 2371.
11. J. Hassoun, Y. Sun, B. Scrosati, *J. Power Sources*, 2011, **196**, 343.

12. Y. Yang, M. T. McDowell, A. Jackson, J. J. Cha, S. S. Hong, Y. Cui, *Nano Lett.*, 2010, **10**, 1486.
13. J. Hassoun, J. Kim, D. Lee, H. Jung, S. Lee, Y. Sun, B. Scrosati, *J. PowerSources*, 2012, **202,** 308.
14. M. Agostini, J. Hassoun, J. Liu, M. Jeong, H. Nara, T. Momma, T. Osaka, Y. Sun, B. Scrosati, *ACS Appl. Mater. Interfaces*, 2014, ***6***, 10924.
15. T. Takeuchi, H. Sakaebe, H. Kageyama, H. Senoh, T. Sakai, K. Tatsumi, *J. Power Sources*, 2010, **195**, 2928.
16. Y. Yang, G. Zheng, S. Misra, J. Nelson, M. Toney, Y. Cui, *J. Am. Chem. Soc*., 2012, **134**, 5387.
17. K. Cai, M. Song, E. J. Cairns, Y. Zhang, *Nano Lett.*, 2012, **12**, 6474.
18. S. Jeong, D. Bresser, D. Buchholz, M. Winter, S. Passerini, *J. Power Sources*, 2013, **235**, 220.
19. Z. Lin, Z. Liu, N. J. Dudney, C. Liang, *Acs nano*, 2013, **7**, 2829,
20. C. Nan, Z. Lin, H. Liao, M. Song, Y. Li, E. J. Cairns, *J. Am. Chem. Soc.* 2014, **136**, 4659.
21. Z. Yang, J. Guo, S. K. Das, Y. Yu, Z. Zhou, H. D. Abrunab, L. A. Archer, *J. Mater. Chem. A*, 2013, **1**, 1433.
22. Z. W. Seh, H. Wang, N. Liu, G. Zheng, W. Li, H. Yao, Y. Cui, *Chem. Sci.*, 2014, **5**, 1396.
23. Z. W. Seh, H. Wang, P. Hsu, Q. Zhang, W. Li, G. Zheng, H. Yao, Y. Cui, *Energy Environ., Sci.*, 2014, **7**, 672.
24. J. Guo, Z. Yang,Y. Yu, H. D. Abruña, L. A. Archer, *J. Am. Chem. Soc.*, 2013, **135**, 763.
25. K, Han, J, Shen, C, M. Hayner, H. Ye, M. C. Kung, H. H. Kung, *J. Power Sources*, 2014, **251**, 331.
26 .F. Wu , H. Kim, A. Magasinski, J. T. Lee, H. Lin, G. Yushin, *Adv. Energy Mater*., 2014, 1400196.
27. Y. Fu, C. Zu, A. Manthiram, *J. Am. Chem. Soc.*, 2013, **135**, 18044.
28. Y. Fu, Y. Su, A. Manthiram, *Adv. Energy Mater*., 2014, **4**, 1300655.
29. L. Chen, Y. Liu, M. Ashuri, C. Liu, L. L. Shaw, *J. Mater. Chem. A*, 2014, **2**, 18026.
30. K. R. Ryan, L. Trahey, B. J. Ingram, A. K. Burrell, *J. Phys. Chem. C*, 2012, **116**, 19724.